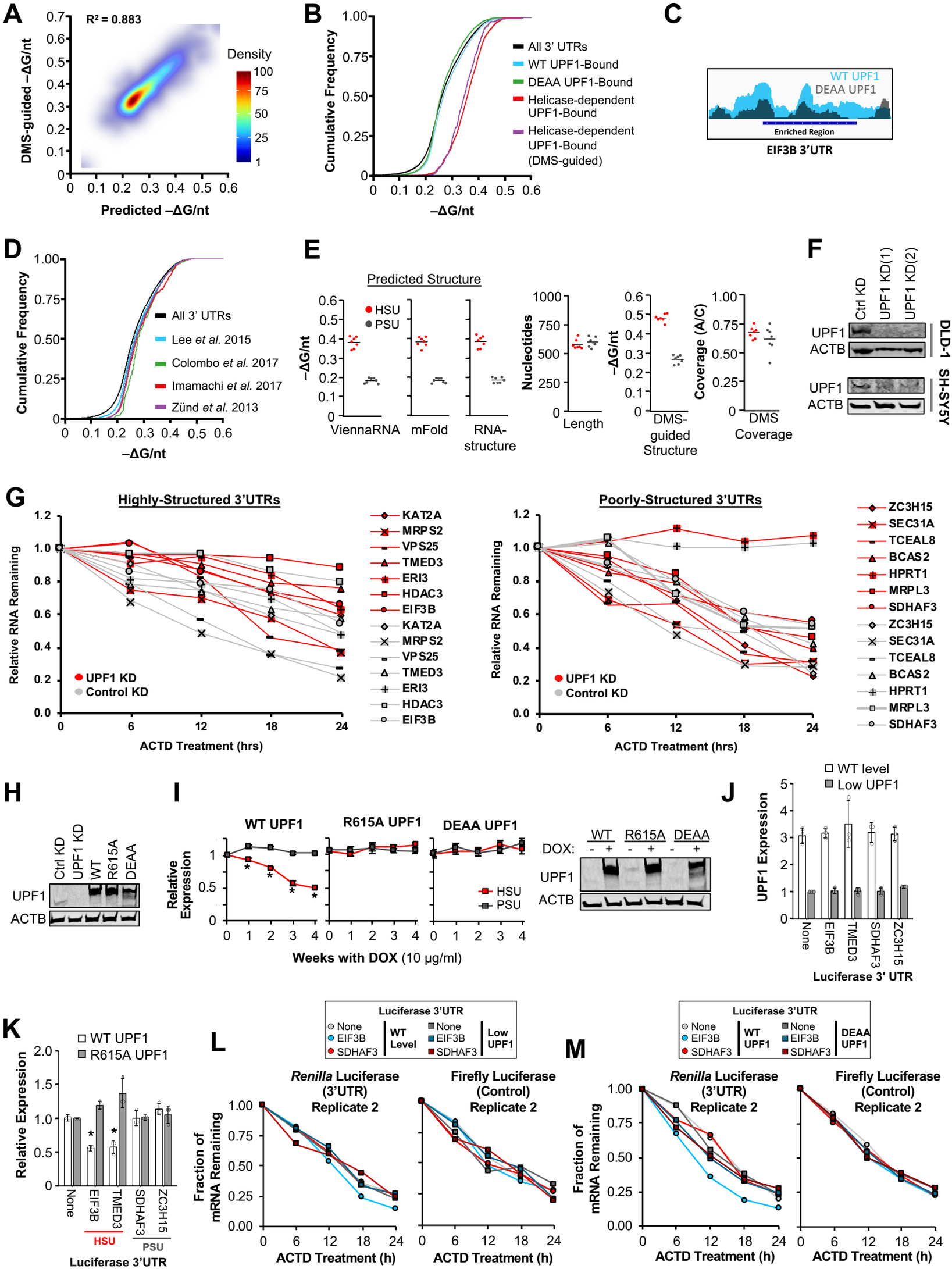
A
R² = 0.883
Density
100
75
50
25
1
DMS-guided –ΔG/nt
Predicted –ΔG/nt
B
Cumulative Frequency
All 3' UTRs
WT UPF1-Bound
DEAA UPF1-Bound
Helicase-dependent UPF1-Bound
Helicase-dependent UPF1-Bound (DMS-guided)
–ΔG/nt
C
WT UPF1
DEAA UPF1
Enriched Region
EIF3B 3'UTR
D
Cumulative Frequency
All 3' UTRs
Lee et al. 2015
Colombo et al. 2017
Imamachi et al. 2017
Zünd et al. 2013
–ΔG/nt
E
Predicted Structure
HSU
PSU
–ΔG/nt
ViennaRNA
mFold
RNA-structure
Nucleotides
Length
DMS-guided Structure
Coverage (A/C)
DMS Coverage
F
Ctrl KD
UPF1 KD(1)
UPF1 KD(2)
UPF1
ACTB
DLD-1
SH-SY5Y
G
Highly-Structured 3'UTRs
Relative RNA Remaining
UPF1 KD
Control KD
ACTD Treatment (hrs)
KAT2A
MRPS2
VPS25
TMED3
ERI3
HDAC3
EIF3B
Poorly-Structured 3'UTRs
ZC3H15
SEC31A
TCEAL8
BCAS2
HPRT1
MRPL3
SDHAF3
H
Ctrl KD
UPF1 KD
WT
R615A
DEAA
UPF1
ACTB
I
WT UPF1
R615A UPF1
DEAA UPF1
Relative Expression
HSU
PSU
Weeks with DOX (10 µg/ml)
DOX:
WT
R615A
DEAA
J
WT level
Low UPF1
UPF1 Expression
None
EIF3B
TMED3
SDHAF3
ZC3H15
Luciferase 3' UTR
K
WT UPF1
R615A UPF1
Relative Expression
None
EIF3B
TMED3
SDHAF3
ZC3H15
HSU
PSU
Luciferase 3'UTR
L
Luciferase 3'UTR
None
EIF3B
SDHAF3
WT Level
Low UPF1
Renilla Luciferase (3'UTR) Replicate 2
Firefly Luciferase (Control) Replicate 2
Fraction of mRNA Remaining
ACTD Treatment (h)
M
Luciferase 3'UTR
WT UPF1
DEAA UPF1
Renilla Luciferase (3'UTR) Replicate 2
Firefly Luciferase (Control) Replicate 2
Fraction of mRNA Remaining
ACTD Treatment (h)

Figure S1 (continued from last page): Helicase-dependent UPF1 regulates mRNAs with highly-structured 3'UTRs, Related to Figure 1. (A) Positive correlation with the coefficient of determination (R^2) calculated between predicted and DMS-guided (Zubradt et al., 2017) overall structure (n = 1,383; Table S2). **(B)** The cumulative distribution function of -ΔG/nt was calculated for all (n = 47,760), WT UPF1-bound (n = 24,110), UPF1 mutant DEAA-bound (n = 23,570), helicase-dependent UPF1-bound (n = 3,036), and helicase-dependent UPF1-bound with DMS-guided coverage (n = 333) 3'UTRs (Table S1 and S2). **(C)** Integrative Genomics Viewer (Robinson et al., 2011) tracks to illustrate helicase-dependent UPF1-bound enriched region of UPF1 CLIP-seq reads for the EIF3B 3'UTR. **(D)** Cumulative distribution function of -ΔG/nt for all 3'UTRs and WT UPF1-bound 3'UTRs from 4 separate studies (Colombo et al., 2017; Imamachi et al., 2017; Lee et al., 2015; Zünd et al., 2013) (n = 24,110, 1,460, 7,700, and 20,138 respectively; Table S1). **(E)** Candidate transcripts were chosen and analyzed for the predicted overall structure (Bellaousov et al., 2013; Lorenz et al., 2011; Zuker, 2003), length, DMS-guided structure, and DMS coverage. **(F)** Western blot analysis of UPF1 knockdown (KD) DLD-1 and SH-SY5Y cells from Figure 1C. **(G)** Degradation of individual candidate mRNAs for the first biological replicate of the 24 h ACTD experiment in Figure 1D. **(H)** Western blot analyses of UPF1 KD cells reintroduced with UPF1 GFP-tagged constructs from Figure 1E. **(I)** Average expression of candidate mRNAs during a UPF1-induction time course. UPF1 KD DLD-1 cells were stably integrated with a DOX-inducible GFP construct using the Flp-In T-Rex system. WT, R615A, and DEAA UPF1-expressing cells were treated with DOX (10 μg/ml) to induce expression at week 0, and cells were passaged every 3-4 days. RNA expression was analyzed every week, and each data point represents the average of 7 candidate mRNAs analyzed by RT-qPCR in triplicate normalized to week 0. Western blot analyses were analyzed following treatment with or without DOX (10 μg/ml) for 48 hours. **(J)** RNA expression of UPF1 from DOX-inducible luciferase experiments from Figure 1F. **(K)** Analysis of *Renilla* luciferase with candidate 3'UTRs in DLD-1 cells that overexpress WT or R615A UPF1 as in Figure 1F. **(L-M)** Second replicates of *Renilla* and Firefly Luciferase RNA half-lives for **(L)** WT compared to low levels of WT UPF1 from Figure 1G and **(M)** WT compared to DEAA UPF1 from Figure 1H. Significant differences (p-value <0.05) were determined by Student's t-tests and denoted with * in panels I and K. Statistics of all RT-qPCR data is documented in Table S5.

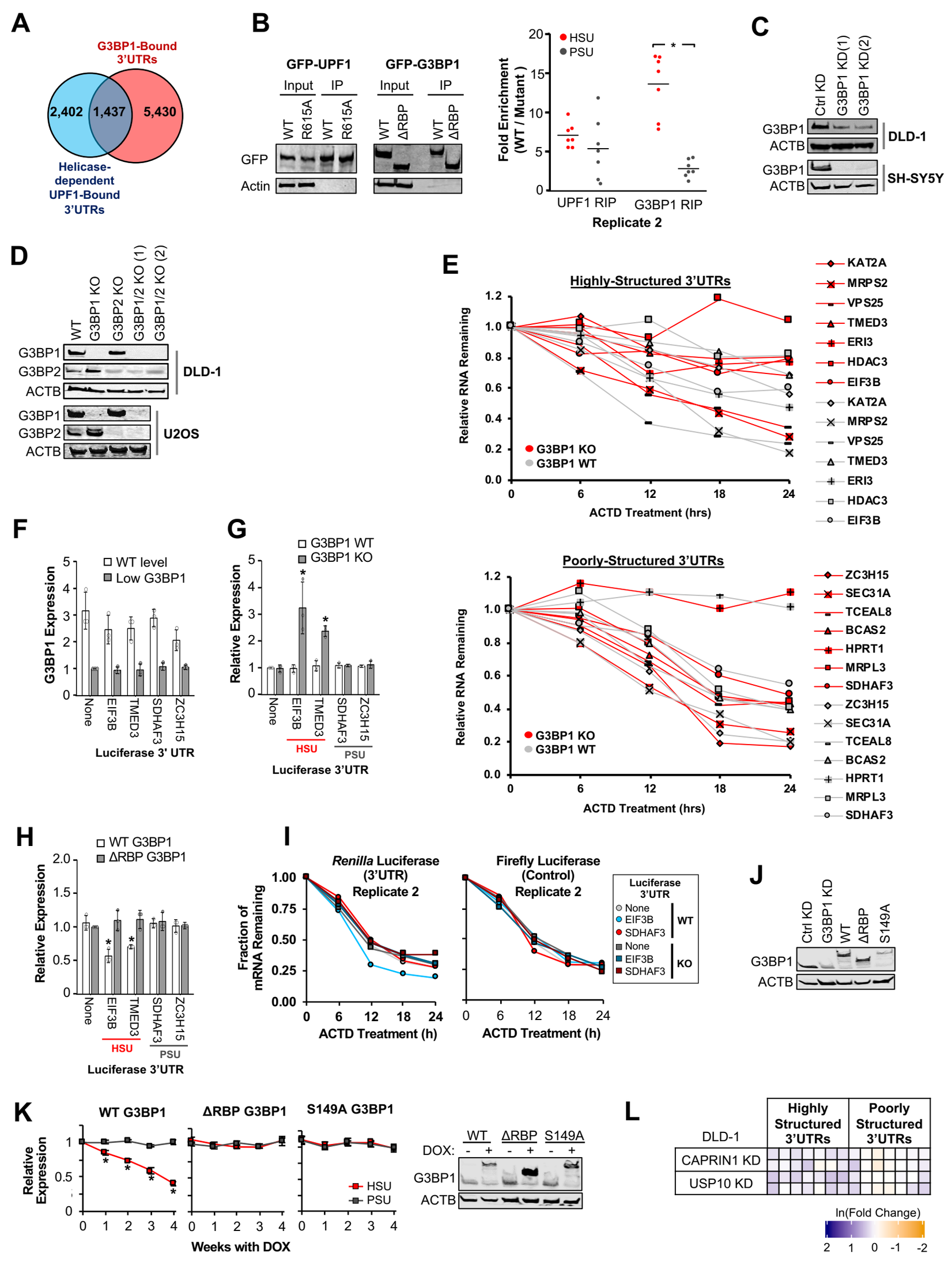
A
G3BP1-Bound 3'UTRs
2,402
1,437
5,430
Helicase-dependent UPF1-Bound 3'UTRs
B
GFP-UPF1
GFP-G3BP1
Input
IP
WT
R615A
ΔRBP
GFP
Actin
HSU
PSU
Fold Enrichment (WT / Mutant)
UPF1 RIP
G3BP1 RIP
Replicate 2
C
Ctrl KD
G3BP1 KD(1)
G3BP1 KD(2)
G3BP1
ACTB
DLD-1
SH-SY5Y
D
WT
G3BP1 KO
G3BP2 KO
G3BP1/2 KO (1)
G3BP1/2 KO (2)
G3BP2
U2OS
E
Highly-Structured 3'UTRs
Relative RNA Remaining
G3BP1 KO
G3BP1 WT
ACTD Treatment (hrs)
KAT2A
MRPS2
VPS25
TMED3
ERI3
HDAC3
EIF3B
Poorly-Structured 3'UTRs
ZC3H15
SEC31A
TCEAL8
BCAS2
HPRT1
MRPL3
SDHAF3
F
WT level
Low G3BP1
G3BP1 Expression
None
EIF3B
TMED3
SDHAF3
ZC3H15
Luciferase 3' UTR
G
G3BP1 WT
G3BP1 KO
Relative Expression
HSU
PSU
Luciferase 3'UTR
H
WT G3BP1
ΔRBP G3BP1
I
Renilla Luciferase (3'UTR) Replicate 2
Firefly Luciferase (Control) Replicate 2
Fraction of mRNA Remaining
ACTD Treatment (h)
Luciferase 3'UTR
None
EIF3B
SDHAF3
WT
KO
J
Ctrl KD
G3BP1 KD
WT
ΔRBP
S149A
G3BP1
ACTB
K
WT G3BP1
ΔRBP G3BP1
S149A G3BP1
Relative Expression
HSU
PSU
Weeks with DOX
DOX:
L
DLD-1
Highly Structured 3'UTRs
Poorly Structured 3'UTRs
CAPRIN1 KD
USP10 KD
ln(Fold Change)

Figure S2 (continued from last page): G3BP1 regulates mRNAs with highly-structured 3'UTRs, Related to Figure 2. (A) Venn diagram illustrating the overlap of 3'UTRs bound by helicase-dependent UPF1 and G3BP1 (Table S1). **(B)** Analysis of RNA immunoprecipitation of GFP-tagged UPF1 and G3BP1. Western blot confirmation of RNA immunoprecipitation and RT-qPCR analysis of a biological replicate of RNA immunoprecipitation as performed in Figure 2B. **(C)** Western blot analysis of G3BP1 KD cell lines from Figure 2C. **(D)** Western blot analysis of G3BP1 and G3BP2 KO cell lines from Figure 2D. **(E)** Degradation of individual candidate mRNAs for the first biological replicate of actinomycin D experiments from Figure 2E. **(F)** RNA expression of G3BP1 mRNA from DOX-inducible luciferase experiments in Figure 2F. **(G)** Analyses of *Renilla* luciferase RNA expression in G3BP1 WT and KO DLD-1 cells as in Figure 2F. **(H)** Analyses of *Renilla* luciferase expression with candidate 3'UTRs in DLD-1 cells that overexpress G3BP1 WT or ΔRBP mutant. **(I)** The second replicate for the change in luciferase RNA half-lives from actinomycin D-treated G3BP1 WT and KO cells as in Figure 2G. All *Renilla* and firefly luciferase expression data in Table S5. **(J)** Western blot analyses of G3BP1 KD cells reintroduced with G3BP1 GFP-tagged constructs from Figure 2H. **(K)** Average expression of candidate mRNAs during a G3BP1-induction time course. G3BP1 KD DLD-1 cells were stably integrated with DOX-inducible WT, ΔRBP, and S149A G3BP1 and analyzed for RNA and protein expression as in Figure S1I. **(L)** DLD-1 cells stably expressing shRNAs targeting G3BP1-associated genes were analyzed for changes in gene expression as in Figure 1C. Significant differences (p-value <0.05) were determined by Student's t-tests and denoted with * in panels B, G, H and K. Statistics of all RT-qPCR data is documented in Table S5.

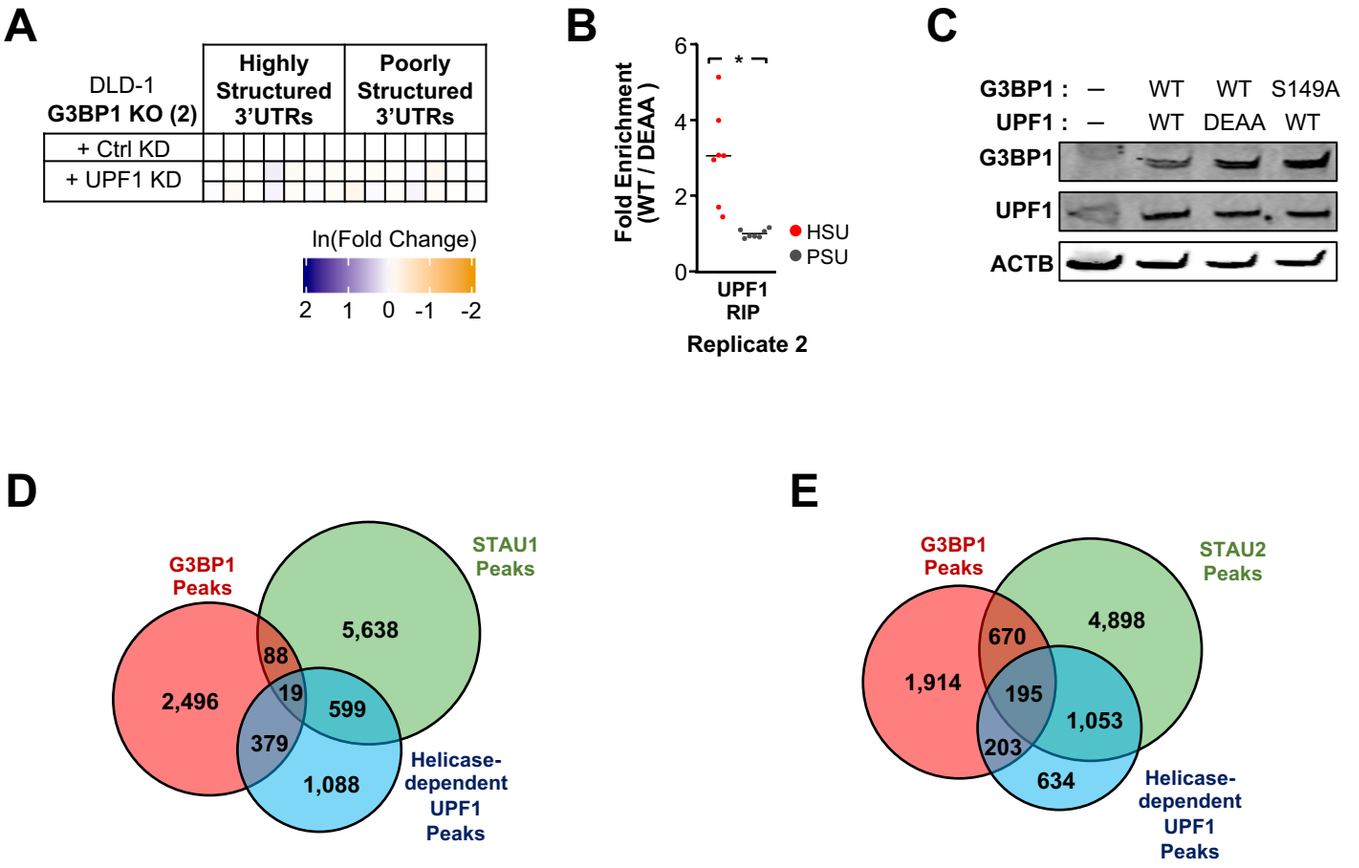

Figure S3: UPF1 and G3BP1 regulate transcripts with highly-structured 3'UTRs through a mechanism independent of other UPF1-associated pathways, Related to Figure 3. (A) Analysis of G3BP1 KO DLD-1 cells using a second gRNA with the additional stable control (Ctrl) KD and UPF1 KD as in Figure 3A. **(B)** The second RT-qPCR replicate of the pulldown of WT and DEAA UPF1 from Figure 3B. **(C)** Analysis of UPF1 and G3BP1 protein expression in transfected G3BP1 KO + UPF1 KD cells from Figure 3C. **(D-E)** Venn diagram illustrating the overlap of 3'UTR CLIP-seq peaks for helicase-dependent UPF1 (Lee et al. 2015) and G3BP1 (Dunham et al. 2012) with **(D)** STAU1 (Sugimoto et al. 2015) or **(E)** STAU2 (Dunham et al. 2012). Significant differences (p-value <0.05) were determined by Student's t-tests and denoted with * in panel B. Statistics of all RT-qPCR data is documented in Table S5

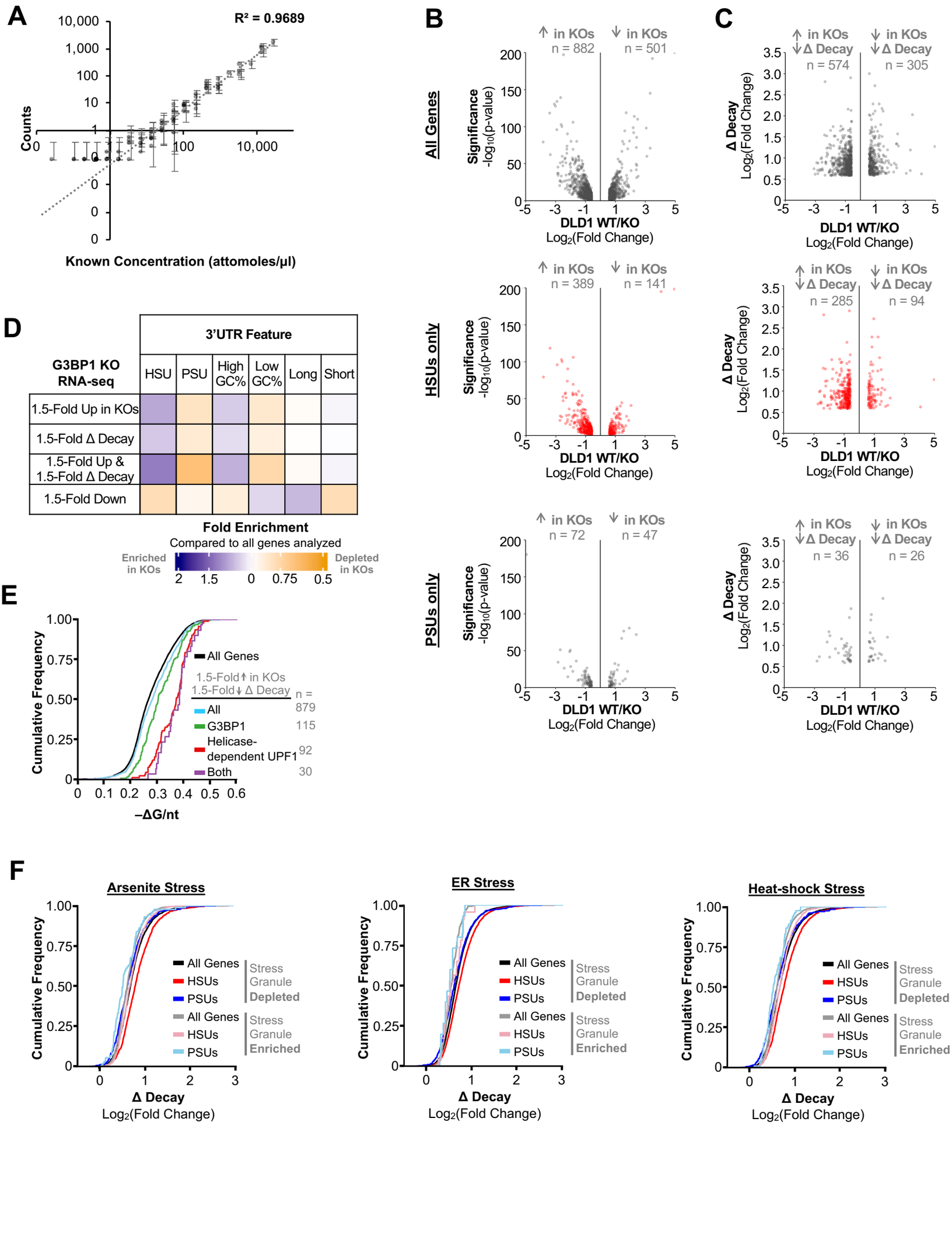
A
R² = 0.9689
Counts
Known Concentration (attomoles/µl)
B
All Genes
HSUs only
PSUs only
↑ in KOs
↓ in KOs
n = 882
n = 501
n = 389
n = 141
n = 72
n = 47
Significance
-log10(p-value)
DLD1 WT/KO
Log2(Fold Change)
C
↑ in KOs ↓Δ Decay
↓ in KOs ↓Δ Decay
n = 574
n = 305
n = 285
n = 94
n = 36
n = 26
Δ Decay
Log2(Fold Change)
D
3'UTR Feature
G3BP1 KO RNA-seq
HSU
PSU
High GC%
Low GC%
Long
Short
1.5-Fold Up in KOs
1.5-Fold Δ Decay
1.5-Fold Up & 1.5-Fold Δ Decay
1.5-Fold Down
Fold Enrichment
Compared to all genes analyzed
Enriched in KOs
Depleted in KOs
2 1.5 0 0.75 0.5
E
Cumulative Frequency
–ΔG/nt
All Genes
1.5-Fold↑ in KOs
1.5-Fold↓ Δ Decay
n =
All 879
G3BP1 115
Helicase-dependent UPF1 92
Both 30
F
Arsenite Stress
ER Stress
Heat-shock Stress
Δ Decay
Log2(Fold Change)
All Genes
HSUs
PSUs
Stress Granule Depleted
Stress Granule Enriched

Figure S4 (continued from last page): G3BP1 preferentially regulates the expression and decay of genes with HSUs globally, Related to Figure 4. (A) Correlation of all ERCC spike-in known concentrations and RNA-seq gene counts with the coefficient of determination (R^2) calculated. **(B)** Volcano plots depicting the fold change and p-values for the differentially expressed genes in G3BP1 WT vs KO cells for all genes, genes with HSUs, and genes with PSUs. **(C)** Volcano plots depicting the change in steady-state levels and decay for the differentially expressed genes in G3BP1 WT vs KO cells for all genes, genes with HSUs, and genes with PSUs. **(D)** Analysis of the enrichment of genes that were differentially expressed and/or decreased decay (1.5-fold) based on different 3'UTR features as in Figure 4B. Corresponding statistics are detailed in Table S3. **(E)** Cumulative distribution function of the average -ΔG/nt for all genes detected, and for all genes, G3BP1-bound, helicase-dependent UPF1-bound, and both-bound genes up-regulated (>1.5 fold) with reduced decay (>1.5 fold) in G3BP1 KO cells. **(F)** Cumulative distribution function of the change in decay in G3BP1 KO cells for genes enriched or depleted in stress granules induced by arsenite stress, ER stress, or heat-shock stress (Namkoong et al., 2018) as in Figure 4E. HSUs with 2-fold decrease in decay were significantly enriched in the stress granule depleted genes (p-value <0.0001 for all three stress conditions).

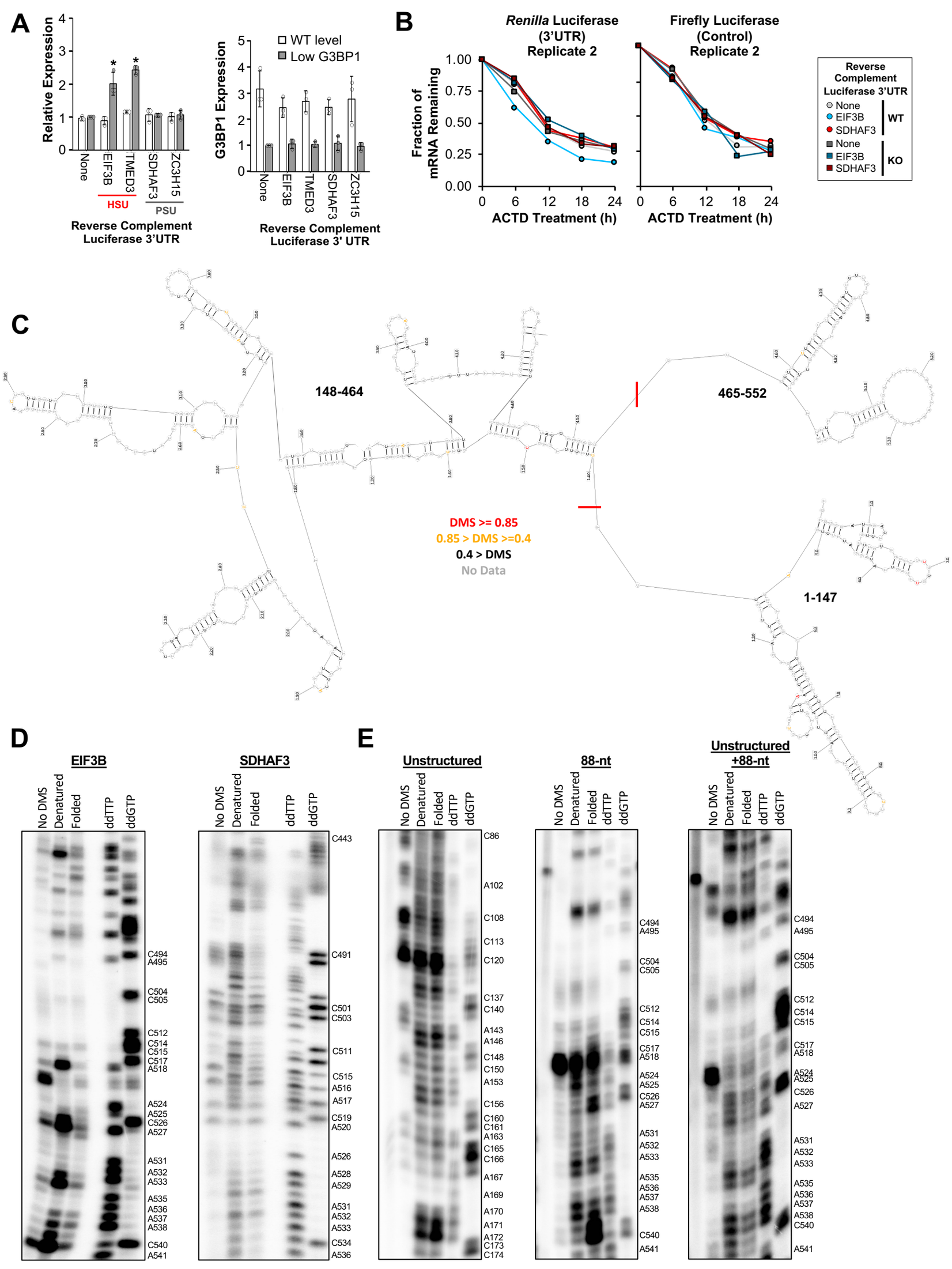
A
Relative Expression
None
EIF3B
TMED3
SDHAF3
ZC3H15
HSU
PSU
Reverse Complement Luciferase 3'UTR
G3BP1 Expression
WT level
Low G3BP1
Reverse Complement Luciferase 3' UTR
B
Renilla Luciferase (3'UTR) Replicate 2
Firefly Luciferase (Control) Replicate 2
Fraction of mRNA Remaining
ACTD Treatment (h)
Reverse Complement Luciferase 3'UTR
None
EIF3B
SDHAF3
WT
KO
C
148-464
465-552
1-147
DMS >= 0.85
0.85 > DMS >=0.4
0.4 > DMS
No Data
D
EIF3B
SDHAF3
No DMS
Denatured
Folded
ddTTP
ddGTP
E
Unstructured
88-nt
Unstructured +88-nt

Figure S5 (continued from last page): SRD regulation is dependent on the overall 3'UTR structure, Related to Figure 5. (A) Analysis of G3BP1-mediated regulation of the reverse complements of 3'UTRs in G3BP1 DOX-inducible cells as in Figure 5B. Significant differences (p-value <0.05) were determined by Student's t-tests and denoted with *. **(B)** The second replicate for the change in reverse complement luciferase RNA half-lives from actinomycin D-treated G3BP1 WT and KO cells as in Figure 5C. **(C)** DMS-MaPseq data was used to guide the folding of the EIF3B 3'UTR. Red lines indicate the location in which EIF3B was divided into thirds for fragment analyses in Figure 3D. **(D-E)** DMS analyses on *in vitro* transcribed 3'UTRs in denatured and folded states for **(D)** EIF3B (HSU), SDHAF3 (PSU), **(E)** artificial unstructured, 88-nt EIF3B fragment, and 88-nt fragment with the unstructured sequence inserted upstream 3'UTRs. Statistics of all RT-qPCR data is documented in Table S5.

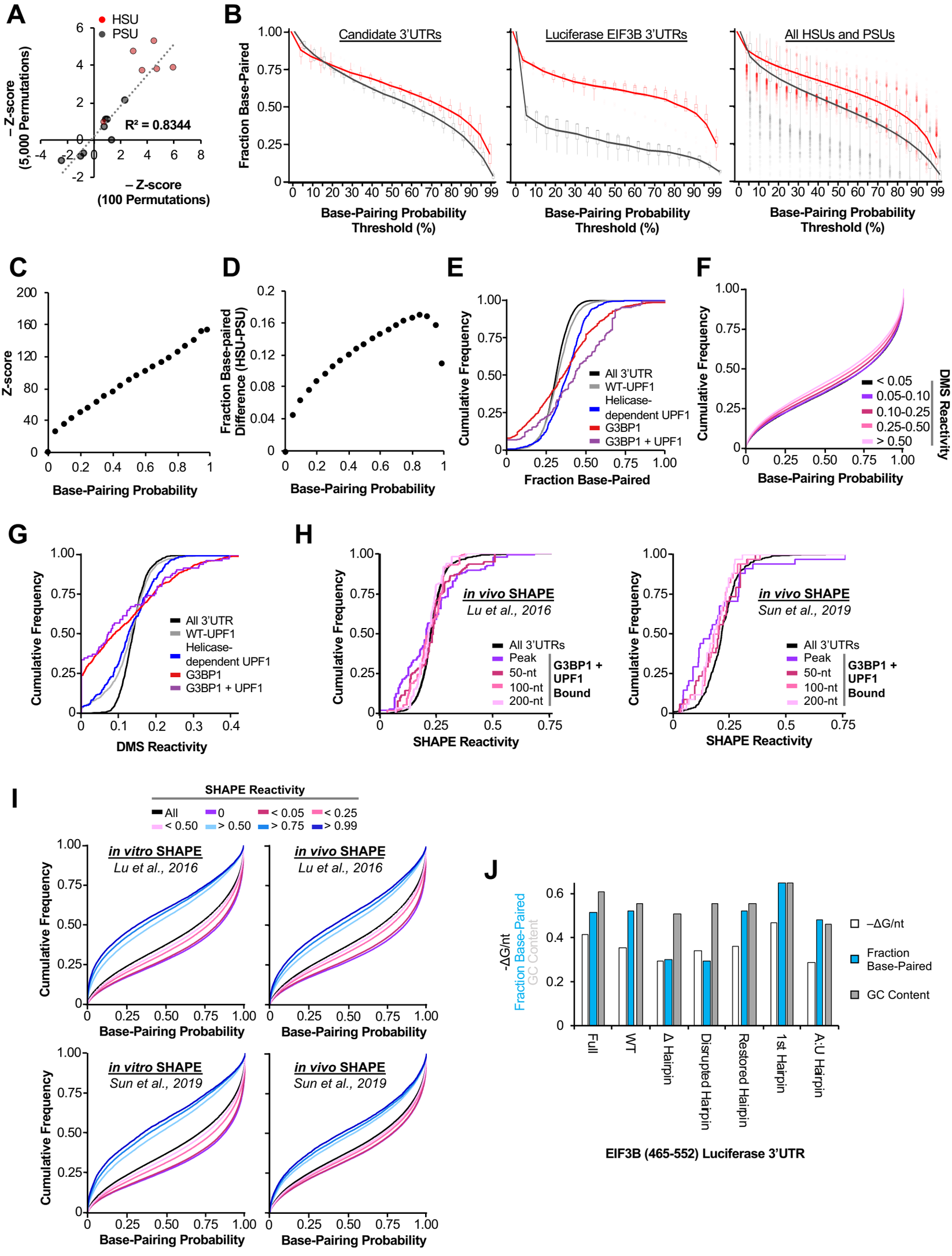
A
HSU
PSU
R² = 0.8344
– Z-score (5,000 Permutations)
– Z-score (100 Permutations)
B
Candidate 3'UTRs
Luciferase EIF3B 3'UTRs
All HSUs and PSUs
Fraction Base-Paired
Base-Pairing Probability Threshold (%)
C
Z-score
Base-Pairing Probability
D
Fraction Base-paired Difference (HSU-PSU)
Base-Pairing Probability
E
Cumulative Frequency
All 3'UTR
WT-UPF1
Helicase-dependent UPF1
G3BP1
G3BP1 + UPF1
Fraction Base-Paired
F
Cumulative Frequency
< 0.05
0.05-0.10
0.10-0.25
0.25-0.50
> 0.50
DMS Reactivity
Base-Pairing Probability
G
Cumulative Frequency
All 3'UTR
WT-UPF1
Helicase-dependent UPF1
G3BP1
G3BP1 + UPF1
DMS Reactivity
H
in vivo SHAPE
Lu et al., 2016
in vivo SHAPE
Sun et al., 2019
All 3'UTRs
Peak
50-nt
100-nt
200-nt
G3BP1 + UPF1 Bound
SHAPE Reactivity
I
SHAPE Reactivity
All
0
< 0.05
< 0.25
< 0.50
> 0.50
> 0.75
> 0.99
in vitro SHAPE
Lu et al., 2016
in vivo SHAPE
Lu et al., 2016
in vitro SHAPE
Sun et al., 2019
in vivo SHAPE
Sun et al., 2019
Cumulative Frequency
Base-Pairing Probability
J
-ΔG/nt
Fraction Base-Paired
GC Content
–ΔG/nt
Fraction Base-Paired
GC Content
Full
WT
Δ Hairpin
Disrupted Hairpin
Restored Hairpin
1st Hairpin
A:U Hairpin
EIF3B (465-552) Luciferase 3'UTR

Figure S6 (continued from last page): SRD regulates highly-base paired structures, Related to Figure 6. (A) Correlation of the z-scores derived by comparing the -ΔG/nt of the actual 3'UTR to the -ΔG/nt for 100 permutations and 5,000 permutations of the 14 candidate 3'UTRs. (B) Boxplots depict the fraction of the entire 3'UTR base-paired with different probability thresholds determined by the partition function in ViennaRNA (Lorenz et al., 2011) for HSUs and PSUs of candidate 3'UTRs, luciferase EIF3B 3'UTRs from Figure 5D-E, and all 3'UTRs. The line plot represents the mean percent of the 3'UTRs being base-paired for each group. (C) Z-score analysis of the difference in base-pairing probability with different thresholds between all HSUs and PSUs. Larger Z-scores represent a more significant difference in the fraction of the 3'UTR base-paired between HSUs and PSUs. (D) The difference in base-pairing between HSUs and PSUs with different base-pairing thresholds. (E) Cumulative distribution function of the fraction of base-paired nucleotides (≥90% probability) for all 3'UTRs, WT UPF1-bound, helicase-dependent UPF1-bound, G3BP1-bound, and G3BP1 + UPF1-bound regions. (F) Cumulative distribution function of the predicted base-pairing probability for individual 3'UTR nucleotides with increasing DMS reactivity cutoffs. (G) Cumulative distribution function of the DMS reactivity for all 3'UTRs, WT UPF1-bound, helicase-dependent UPF1-bound, G3BP1-bound, and G3BP1 + UPF1-bound regions. (H) Cumulative distribution function of SHAPE reactivity from Lu et al. (2016; Top panel) and Sun et al. (2019; Bottom panel) for G3BP1 + UPF1-bound regions (peak and its surrounding 0, 100, and 200 nts with the peak as the mid-point). (I) Cumulative distribution function of the predicted base-pairing probability for individual 3'UTR nucleotides with different in vitro and in vivo SHAPE reactivity cutoffs from Lu et al. (2016; Top panels) and Sun et al. (2019; Bottom panels). (J) Analysis of the overall structure, fraction base-paired (>90%), and GC content for the resulting mutations of the 88-nt EIF3B fragment from Figure 6H.

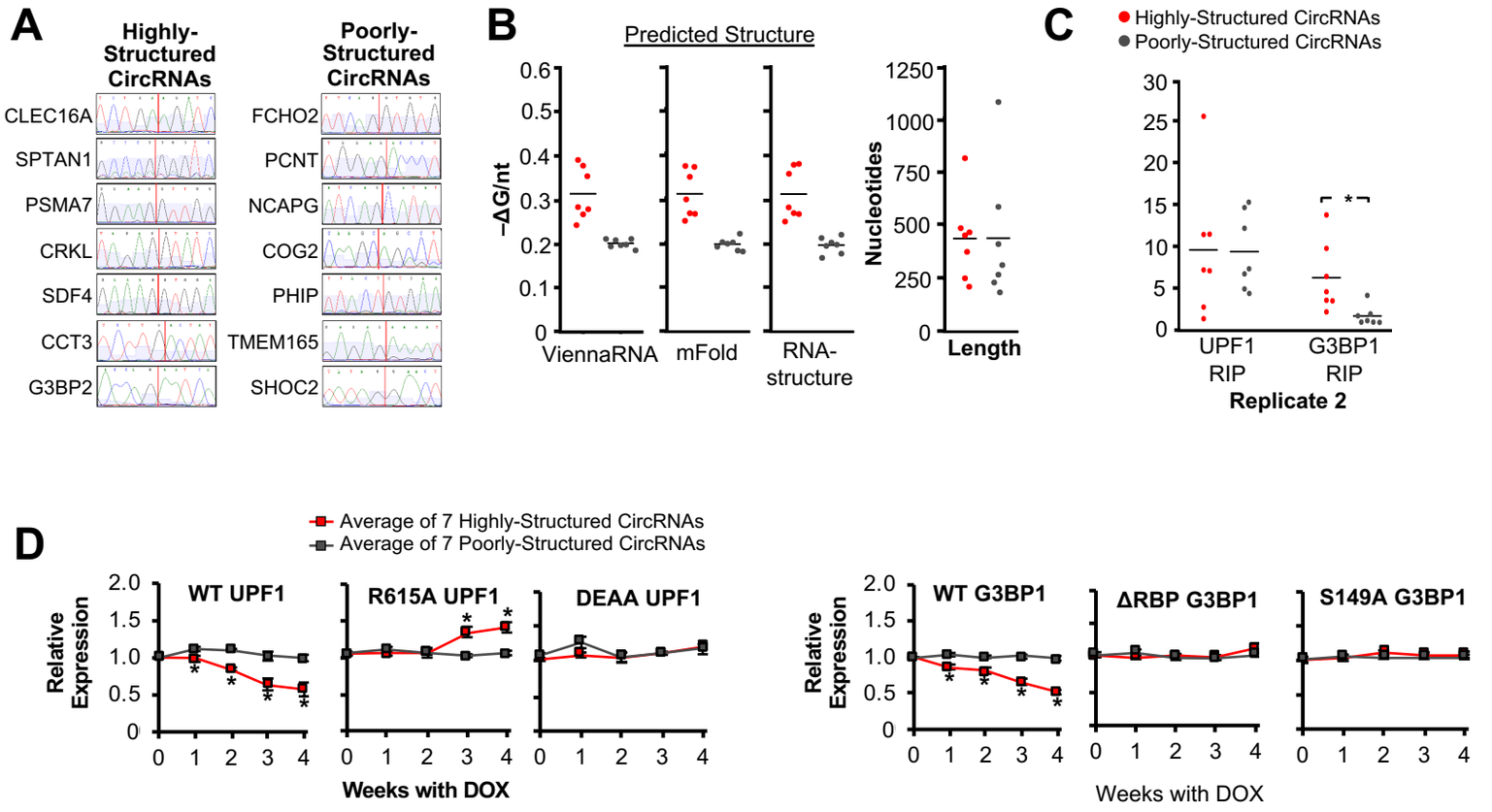

Figure S7: UPF1 and G3BP1 differentially regulate circRNAs, Related to Figure 7. (A) Validation of circRNA RT-qPCR products by Sanger sequencing for 7 highly-structured and 7 poorly-structured candidate circRNAs. 10 nucleotides surrounding the circRNA back-splice junction was shown to confirm the identity of the RT-qPCR products. **(B)** Candidate circRNAs were analyzed for predicated overall structure and length. Three folding programs were used to determine the overall structure (Bellaousov et al., 2013; Lorenz et al., 2011; Zuker, 2003). **(C)** The RNA immunoprecipitations performed in Figure 2B and S2B were analyzed for candidate circRNA association. **(D)** Average expression of candidate circRNAs during a UPF1 and G3BP1 DOX-induction time course as in Figure S1I and S2K. Significant differences (p-value <0.05) were determined by Student's t-tests and denoted with * in panels C and D. Statistics of all RT-qPCR data is documented in Table S5.